Surface & Coatings Technology 364 (2019) 115–126

Contents lists available at ScienceDirect

Surface & Coatings Technology

journal homepage: www.elsevier.com/locate/surfcoat

Laser metal deposition of vanadium-rich high speed steel: Microstructural and high temperature wear characterization

N. Ur Rahman[a,*], L. Capuano[a], M.B. de Rooij[b], D.T.A. Matthews[a,c], A. Garcia-Junceda[d], M.A. Mekicha[b], L. Cordova[e], G. Walmag[f], M. Sinnaeve[g], G.R.B.E. Römer[a]

[a] Chair of Laser Processing, Department of Mechanics of Solids, Surfaces & Systems (MS 3), Faculty of Engineering Technology, University of Twente, Enschede, the Netherlands
[b] Chair of Surface Technology & Tribology, Department of Mechanics of Solids, Surfaces & Systems (MS 3), Faculty of Engineering Technology, University of Twente, Enschede, the Netherlands
[c] Chair of Skin Tribology, Department of Mechanics of Solids, Surfaces & Systems (MS 3), Faculty of Engineering Technology, University of Twente, Enschede, the Netherlands
[d] IMDEA Materials Institute, C/Eric Kandel 2, Getafe 28906, Madrid, Spain
[e] Chair of Dynamics Based Maintenance, Department of Mechanics of Solids, Surfaces & Systems (MS 3), Faculty of Engineering Technology, University of Twente, Enschede, the Netherlands
[f] CRM Group, Metal Processing Technology, Rue des Ples 1 B56-Quartier Polytech 2, Liege B-4000, Belgium
[g] Marichal Ketin, Rue Ernest Solvay 372, Liege 4000, Belgium

ARTICLE INFO

Keywords:
High speed steel
Laser metal deposition
Microstructural refinement
Hot metal forming
Carbide morphology
Oxidative wear

ABSTRACT

A comparative high temperature wear study was conducted between two alloys: laser metal deposited vanadium-rich (V-rich) high speed steel (HSS) and spun cast carbide enhanced indefinite chilled double poured (CE-ICDP) iron. Laser Metal Deposition (LMD) of V-rich HSS alloy was performed by using a 4.0 kW Nd:YAG laser at three different laser scan speeds to investigate the effect thereof on the carbide size and morphology, phase constitution and mechanical properties (such as micro-hardness and wear resistance) of the laser metal deposits.

A comprehensive microstructural characterization of these alloys revealed that the dendritic microstructure of the V-rich HSS alloy consisted of martensitic matrix and VC carbides. Increasing the laser processing speeds significantly changed the morphologies of VC carbides from square and round to angular and rod-like shapes. The micro-hardness of the V-rich HSS was improved from 760 HV to 835 HV by increasing the laser processing speed. During high temperature (500 °C) pin-on-disc wear tests, the V-rich HSS showed excellent wear resistance compared to CE-ICDP iron. It was found that V-rich HSS with square and round shape VC carbides (V-rich 10 mm/s) showed the most improved tribological performance with oxidative wear found to be the dominant wear mechanism at this temperature.

1. Introduction

In hot metal forming processes (e.g. hot stamping, moulding and extrusion), tools undergo severe working conditions due to extreme cyclic thermo-mechanical loads combined with abrasion, adhesion and tribo-oxidation [1]. This results in the degradation of surfaces and excessive wear, which affect the product quality and limit the life of the tool [2]. High speed steel (HSS) alloys have become a favorable choice for such applications due to their excellent mechanical properties (high micro-hardness, high strength and ductility, and good tempering resistance) at elevated temperatures [3,4]. HSS alloys are characterized by fine hard carbides (MC, M_2C, M_6C, M_7C_3 and $M_{23}C_6$) and a martensitic matrix [5]. The mechanical properties of the HSS alloys are highly influenced by microstructural features such as type, morphology, volume fraction and distribution of the carbides, as these carbides significantly contribute to mechanical strength, load bearing capability and wear resistance during high temperature tribological contacts [6].

HSS alloys are currently produced by conventional production methods such as casting and forging [7]. The production through casting has inherent limitations on resulting microstructure and mechanical properties. Slow cooling rates during casting results in coarse microstructure, which limits the most desired thermo-mechanical fatigue strength [8]. There is a limited freedom in selecting the alloys composition in casting due to segregation of carbides [9]. It is

* Corresponding author at: P.O. Box 217, 7500 AE Enschede, the Netherlands
E-mail address: n.naveedurrahman@utwente.nl (N.U. Rahman).

https://doi.org/10.1016/j.surfcoat.2019.02.044
Received 20 December 2018; Received in revised form 11 February 2019; Accepted 15 February 2019
Available online 27 February 2019

significantly important to increase the matrix hardness by increasing the phase fraction of homogeneously distributed optimum sized hard carbides to resist the wear caused by the hard oxide layer of the counter material at high temperatures [10,11]. At the same time, refinement of the microstructure is necessary to sustain the extreme cyclical thermal loads. To overcome the limitations of the casting process, adoption of alternate production routes is required which should provide superior control of cooling rates to refine the microstructure and provide freedom in material/alloy choice [12].

Laser metal deposition (LMD) is a laser-based powder blown technique, which uses laser energy to deposit clad layers of enhanced properties onto the substrate [13]. In the LMD technique, the reported cooling rates are up to 10^3 and 10^4 K/s [14]. Such high cooling rates result in refining of the microstructure with improved mechanical properties such as micro-hardness, tensile and fatigue strengths [15,16]. LMD with powder injection is found to be the most effective as it provides liberty to vary the chemical composition of powder materials according to desired mechanical properties [17].

The purpose of the present study is to employ laser-based powder blown technique (LMD) for the production of HSS coatings for hot metal forming systems; to overcome the limitations faced during conventional manufacturing (e.g. casting). In previous research, it was observed that LMD HSS alloys showed inferior wear resistance at high temperature due to partial oxidation of matrix and carbides [18], which was predominantly due to the type and morphology of the carbides present [19]. In the current paper, LMD of V-rich HSS was performed by varying the laser scanning speed; to study the effect of high cooling rates on the microstructure and the morphology of carbides. The purpose of depositing V-rich HSS powder was to precipitate large phase fraction of VC carbides in the matrix, as VC carbides are highly prone to oxidation [20] and are also highly wear resistant due to their morphology and high micro-hardness [21]. Friction and wear characterization of V-rich HSS alloys was performed by using a high temperature pin-on-disc tribometer and compared with that of conventionally cast carbide enhanced indefinite chilled double poured (CE-ICDP) iron. The reason for selecting CE-ICDP iron as a reference for this comparative study is its well known lubricious properties in high temperature tribological contacts [22]. High temperature wear tests were carried out at 500 °C which is an average high temperature of metal forming contacts [18,23]. The effect of morphology, size and phase fraction of VC carbides on the friction and wear was investigated.

2. Experimental

2.1. Experimental setup and processing parameters

LMD of V-rich HSS alloy was performed on 50 mm diameter $42CrMo_4$ steel cylindrical substrate by using a 4 kW cw Nd:YAG laser source (Trumpf) equipped with a transport fibre of 600 μm core diameter. The optical head consisting of a 200 mm collimation lens and a 300 mm focal lens, which was mounted to the end-effector of a six degree of freedom ABB robot IRB-2600M2004. For the manipulation of cylindrical substrates, an ABB tilt rotation manipulator was used. The distance between the focusing optic and the substrate was fixed at 340 mm to acquire the beam spot size of 5 mm.

HSS powder from a Twin150C Oerlikon-Metco powder feeder was injected into the laser induced melt-pool on the substrate by using a lateral nozzle (ILT-Fraunhofer) of 2.5 mm diameter. Argon was used as powder carrier gas and for the shielding of the laser deposits from oxidation during LMD. The high power LMD setup is same as shown in [24].

Processing parameters for LMD of V-rich HSS are listed in Table 1. LMD was performed at three different laser scanning speeds (5, 10 and 15 mm/s). V-rich HSS laser deposited at 5 mm/s, 10 mm/s and 15 mm/s are referred to in this paper as V-rich 5V, V-rich 10V and V-rich 15V respectively. LMD of the clad tracks was performed by maintaining a clad overlapping ratio of 45% of the width of a single track.

Table 1
Processing window for the laser cladding process.

Laser power (W)	Laser scan speed (mm/s)	Powder mass flow rate (g/min)	Tracks overlap (%)
1900–3200	5, 10 & 15	11–18	45

Table 2
Experimental conditions for pin-on-disc tests.

Temperature (°C)	Load (N)	Contact pressure (MPa)	Disc speed (m/s)	Distance (m)
500	5	795	0.45	2000

A CSM-Instruments high temperature pin-on-disc tribometer was used to characterize the LMD V-rich HSS and Spun cast CE-ICDP iron. Hemispherical pins of 10 mm diameter were machined from the laser deposits and the cast samples by using a wire Electric Discharge Machining (EDM). Low carbon steel discs of 50 mm diameter were used as the counter surface. Both the pins and discs were polished to an initial surface roughness (Ra) of ≈0.10 μm. During the wear tests, low carbon steel discs were first heated up to 500 °C and later the pin was brought in contact with disc to start the wear tests. The experimental conditions for the high temperature pin-on disc tests are listed in Table 2.

The wear rates were determined from the volume loss of the pins which is calculated from the wear scar diameter [25–27] as

$$V = \frac{\pi d^4}{64R} \tag{1}$$

$$k = \frac{V}{SF_n} \tag{2}$$

in which V represents the volume loss (mm^3) of the pin, d is the wear diameter (mm) of the pin, R is the radius of the pin tip, k represents the wear rate (mm^3/N·m) and it is defined as the volume loss V (mm^3) per unit of the sliding distance S (mm) and of the applied force F_n (N).

2.2. Materials

The chemical compositions of LMD V-rich HSS and spun cast CE-ICDP iron are listed in Table 3. LMD powder was purchased from Carpenter Technology Corporation.

The SEM micrograph of the V-rich HSS powder showed that it consisted of asymmetric particles with satellites present and an average powder particle size of 70 μm, see Fig. 1. Apart from analyzing the morphology of powder particles, moisture content was estimated following a mass loss measurement upon drying the powder using the moisture analyzer MS-70 of A&D Ltd. The sample was placed on a heating plate for 20 min at the temperature of 150 °C following heating at a rate of 10 °C/min. In addition, by using the standard Hall flowmeter method (ASTM B213), the powder flow rate Φ_{Hall} was determined for as-received and dried powders. The difference in the flowability of the moist and dry powders was not substantial, see Fig. 1.

Table 3
Chemical composition of alloys (wt%).

Powders	C	Cr	Mo	V	W	Mn	Si	Ni	Fe
V-rich HSS	1.8–2.2	5.2	1.2	9.0–12.0	0.3	–	1.0	–	bal
CE-ICDP	3.0–4.0	2.0–4.0	0.3	0.2	–	0.8	1.0	4.0	bal

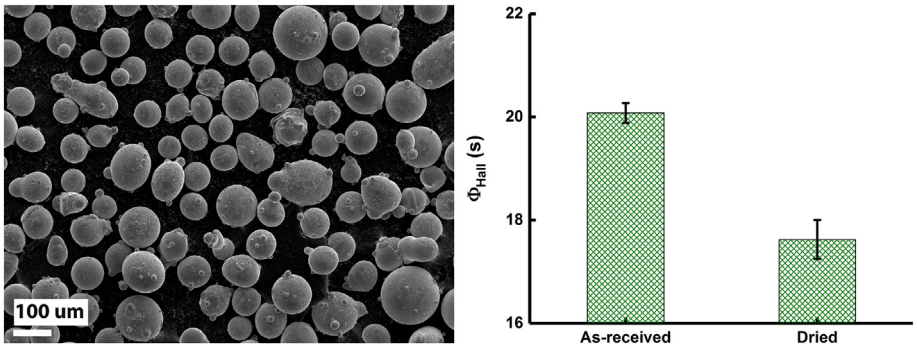

Fig. 1. (L) SEM micrographs showing the morphology of the as-received V-rich HSS powder, (R) plot showing the influence of moisture on the powder flowability of the V-rich HSS powder.

2.3. Analysis tools

Samples for the microstructural analysis were prepared from the cross-sections of LMD bars and were hot-mounted in Bakelite (Struers-PolyFast). Polishing of the samples was performed on Struers TEGRA-MIN-30 by using diamond suspensions of 9 μm, 3 μm, 1 μm, and 0.25 μm, and colloidal silica suspension of 0.04 μm. A JEOL JSM-7200F field emission SEM equipped with Energy Dispersive Spectroscopy (EDS) and Electron Backscattered Diffraction (EBSD) sensors was used for microstructural, elemental and phase analysis which are quantified using AZtecHKL software from Oxford Instruments. X-ray Diffraction (XRD) patterns were obtained by means of the Cu k-alpha radiation of an Empyrean PANalytical diffractometer.

A KEYENCE VHX-5000 optical microscope was used for the measurement of the wear diameter of the pins. A SENSOFAR S-neox non-contact 3D surface profiler was used to measure the surface roughness of the pin and disc samples. The micro-hardness of the cast and LMD alloys was determined by a Leco LM-100AT Vickers indenter. The micro-hardness measurements were conducted at a load of 500 g with a dwell time of 15 s (DIN EN ISO 6507-1 standard) with a minimum of 3 measurements per data point.

3. Results

3.1. Multilayer laser deposits

The laser processing parameters were optimized by depositing single layer tracks with minimal dilution (≤5%) with the substrate, limited amount of porosity, surface oxidation and un-melted powder particles see Fig. 2a and b. The laser processing speed was varied to modify the microstructure due to enhanced cooling. It was found that laser deposition at room temperature resulted in cold cracking upon solidification, see Fig. 2c. To overcome cold cracking, LMD was performed at a pre-heating temperature of 150 °C, which also improved the powder catchment efficiency. In order to observe the effect of sequential laser deposition on tempering of martensite, double layer laser clads (to maximum thickness of 3 mm) were produced, see Fig. 2d.

3.2. Microstructural investigation

Backscattered Electron (BSE) micrographs of the cross-sections of V-rich HSS and CE-ICDP iron are shown in Fig. 3. LMD V-rich HSS consists of typical dendritic microstructure, see Fig. 3a–c. The matrix consists of martensite and retained austenite with primary and secondary carbides at the grain boundaries. The morphology of these carbides are square, round, rod-like and angular. It can be seen that the size of these carbides decreases with increase in the laser scan speed from 5 mm/s to 15 mm/s. The morphology of the carbides are square and rod shape in the LMD V-rich HSS deposited at 5 mm/s but could be modified to mainly rod-like and angular carbides in the LMD V-rich HSS deposited at 15 mm/s. Fig. 4a shows the elemental distribution in the V-rich HSS. EDS analysis revealed that the carbides formed are predominantly enriched with V but Mo and Cr also form part of carbides.

The microstructure of the cast CE-ICDP iron consists of a martensite matrix, coarse carbides M_3C type-Fe_3C (cementite-white), free graphite and secondary carbides along with residual austenite [28,29], see Fig. 3d. The distribution of Ni, Si and C in the CE-ICDP iron revealed by EDS mapping as given in Fig. 4b.

XRD analysis of the LMD and cast materials is shown in Fig. 5. For the LMD V-rich HSS alloys, the carbides peak show the presence of VC, V_8C_7, Mo_2C and Cr_7C_3. The V_8C_7 carbides are also historically referred to as VC carbides [30]. The intensity of the peaks for all three cases of LMD V-rich HSS are almost similar which shows that phase fractions of matrix and carbides have not change much from one case to another. For the CE-ICDP iron, as expected Fe_3C cementite peaks were detected, but on the contrary no peaks for the graphite was found. For graphite the highest peak should appear around 26.5° but no peak was detected during the complete 2θ scan, from 10° to 120°. This could be due to the presence of a very small amount of graphite.

Phase constitutions of the V-rich HSS alloy and CE-ICDP iron determined by EBSD analysis are listed in Table 4. Due to crystallographic similarity, the residual austenite and VC are indexed together. It is found that for LMD V-rich HSS alloy (after martensite) VC carbides account for the larger portion of the microstructure (20–25%). No Fe-V intermetallic compounds were detected, indicating no interdiffusion of V and Fe [31]. For CE-ICDP iron, the larger proportion after the martensitic matrix is of cementite Fe_3C (18–19%). The percentage phase fraction of graphite is 1–2% and is also not homogeneously distributed. For the similar reasons during the XRD analysis, graphite peak could not be detected.

Fig. 6a–c show the phase map and inverse pole figures (IPF) of LMD V-rich HSS respectively. Phase map shows the distribution of carbides (VC and Mo_2C) at the grain boundaries and within the matrix. Grains orientations are found to be heterogeneous in the IPF. The pole figure (PF) of martensite (Fe-BCC) at (100), (110) and (111) planes confirmed no preferential texture orientation of Fe-BCC, see Fig. 6d. Similarly, Fig. 7a–c shows the phase map and IPF of CE-ICDP iron respectively. This phase map shows the presence of coarse Fe_3C carbides and free graphite while the IPF shows the randomly oriented grains in the cast alloy as well.

3.3. Micro-hardness

The micro-hardness of the LMD V-rich HSS (5, 10 and 15 mm/s) was determined from the as-clad double layer laser deposits. The micro-hardness (HV 0.5) measurements showed an increase in the micro-hardness with the increase in the laser processing speed. The maximum measured micro-hardness was 835 ± 20 HV. During the sequential laser deposition, the micro-hardness of the previously deposited layer dropped to 620 ± 20 HV for V-rich HSS deposited at 5 mm/s. The

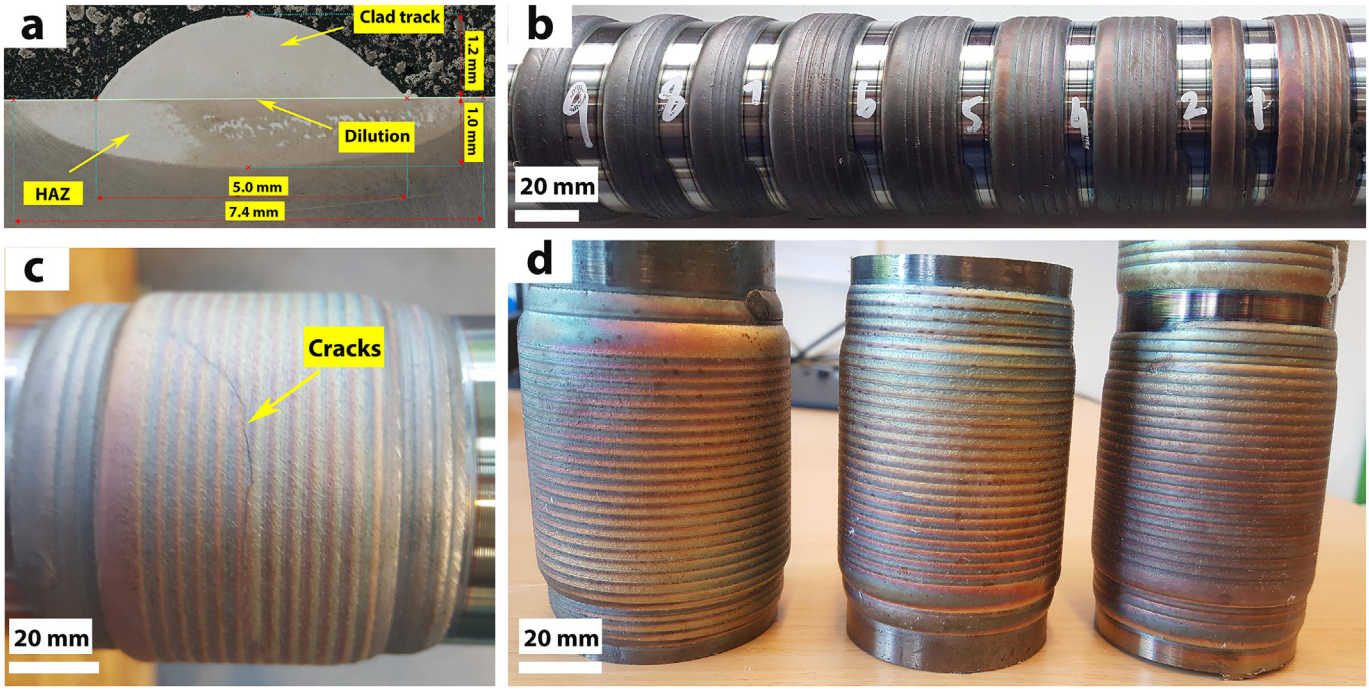

Fig. 2. Photographs of single and multilayer laser depositions. (a) Cross section of a single clad track of V-rich HSS deposited at 10 mm/s showing laser clad, dilution and HAZ, (b) optimization of laser processing window, (c) cracking of double layer sample deposited at room temperature and (d) 2 layers deposits of V-rich HSS produced at 5, 10 & 15 mm/s with a pre-heating temperature of 150 °C.

micro-hardness plot of the V-rich HSS along the clad height is shown in Fig. 8a. Optical image of two overlapping laser clads is shown in Fig. 8b, whereas SEM image of the layers interface region (Fig. 8c) shows the homogeneous distribution of the carbides, with the presence of no defect in the interface region thus ensuring a strong bonding. The maximum measured micro-hardness of the cast CE-ICDP iron was 650 ± 10 HV. It is important to mention that the amount of graphite increases with the decrease in the work roll radius, resulting in a

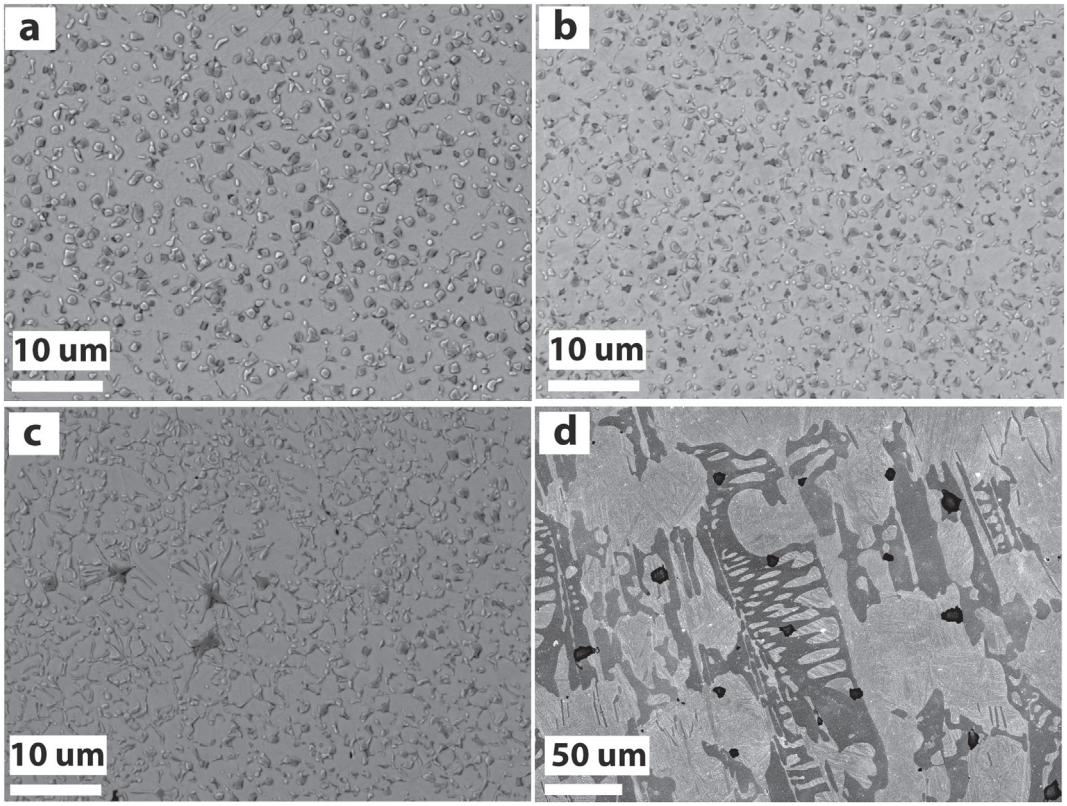

Fig. 3. BSE micrographs showing the highly refined microstructure of LMD. (a) V-rich HSS 5 mm/s, (b) V-rich HSS 10 mm/s, (c) V-rich HSS 15 mm/s and coarse grain structure of cast (d) CE-ICDP iron.

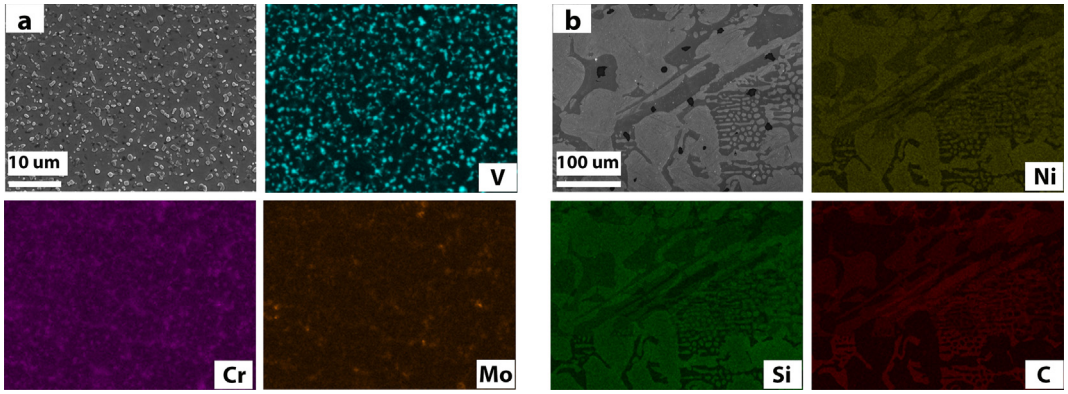

Fig. 4. (a) BSE micrograph of V-rich LMD alloy with EDS elemental mapping showing the carbides mainly enriched with V, (b) BSE micrograph of the cast CE-ICDP with EDS elemental mapping showing distribution of Ni, Si and C.

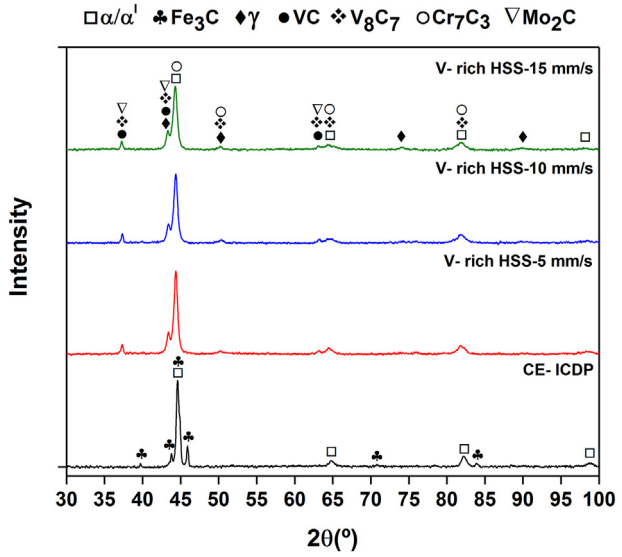

Fig. 5. XRD analysis of the V-rich HSS alloys and CE-ICDP iron showing the presence of different phases.

Table 4
Phase constitution of alloys by EBSD analysis (wt%).

Materials	Martensite	VC	Mo_2C	Cr_7C_3	Fe_3C	Graphite
V-rich HSS-5V	75	20	2	3	–	–
V-rich HSS-10V	75	20	2	3	–	–
V-rich HSS-15V	70–75	20–25	2	3	–	–
CE-ICDP	80	–	–	–	18–19	1–2

reduction of micro-hardness [29].

3.4. Friction and wear

The friction signals recorded for the LMD V-rich HSS and cast CE-ICDP iron during the high temperature pin-on-disc tests at 500 °C are shown in Fig. 9. For the clarity of the data, the friction signal for V-rich HSS 15 mm/s are not shown as these are found similar to that of V-rich HSS 5 mm/s. Mean coefficient of friction for the LMD V-rich HSS alloys are ≈0.55–0.6, which are higher when compared to CE-ICDP iron (≈0.5) at 500 °C.

At the start of the test, the pins were brought into contact with the pre-oxidized surface of low carbon steel disc (heated up to 500 °C) and the sliding was immediately started. For the LMD V-rich alloys, a short running-in was observed as compared to the CE-ICDP iron. Among the LMD, only V-rich HSS 10 mm/s showed a stable coefficient of friction while the other two cases of LMD showed noise in the friction signals. In the case of CE-ICDP iron, similar fluctuations (noise) in the friction signal were observed throughout the tests.

Fig. 9 shows the wear rate of both cast and LMD alloys at 500 °C. The cast CE-ICDP iron showed 3–4 higher wear rate when compared to the LMD V-rich HSS alloys. Wear tests performed at 500 °C showed that wear is mainly driven by oxidative wear. During the wear process, abrasive particles consisting of oxide and metallic debris abraded the matrix of all of the alloys. Adhesion of oxide layer and metal debris to the pin surfaces was observed both for cast and LMD alloys, see Fig. 10.

Among the LMD HSS, V-rich HSS 5 mm/s showed the lowest wear rate while the V-rich 15 mm/s showed the highest wear rate. During the wear tests, when the pin was brought in contact with the pre-oxidized surface of the counter surface, the hard oxide layer wore the matrix and remained in contact with the VC carbides. VC carbides showed good load carrying capability by supporting the counter surface. During which the matrix was oxidized and later VC carbides were also oxidized in accordance with the previous studies which showed these carbides to be highly prone to oxidation [32]. Although the whole worn surface of V-rich HSS alloy was oxidized, an agglomeration of oxide scale was found at the center of the wear scars, see Fig. 10b and c. EDS analyses performed away from the center (Fig. 11) and at the center of worn surface (Fig. 12) showed that presence of oxygen contents of 8% and 17% respectively. Carbides were found to be strongly embedded in the matrix as no carbide pull-out was seen in the analysis of worn surfaces.

Fig. 13 shows the SEM micrograph of the worn surface of the CE-ICDP iron and the EDS analysis. The cast CE-ICDP iron showed the highest wear during the high temperature wear tests. Clear abrasion scratches were found on the matrix, while the adhesion of metallic and oxide debris was also observed. EDS analysis shows no considerable oxide layer formation on the matrix of CE-ICDP iron, see Fig. 13.

3.5. Surface topography

A qualitative surface roughness analysis of the LMD V-rich HSS, CE-ICDP iron and counter discs is presented in Fig. 14. Measured surface roughness Ra value of the V-rich HSS at the center of the wear scar (oxide agglomerated region) is ≈0.55 μm while away from the center is ≈0.14 μm. Removal of the oxide layer from the center of counter surface to V-rich HSS is observed, see Fig. 14b.

Surface roughness profile of CE-ICDP iron showed presence of abrasion marks on the entire worn surface. Measured surface roughness Ra value of the CE-ICDP iron is ≈1.42 μm. Counter surface to the CE-ICDP iron showed a continuous oxide layer with few abrasion marks, see Fig. 14d.

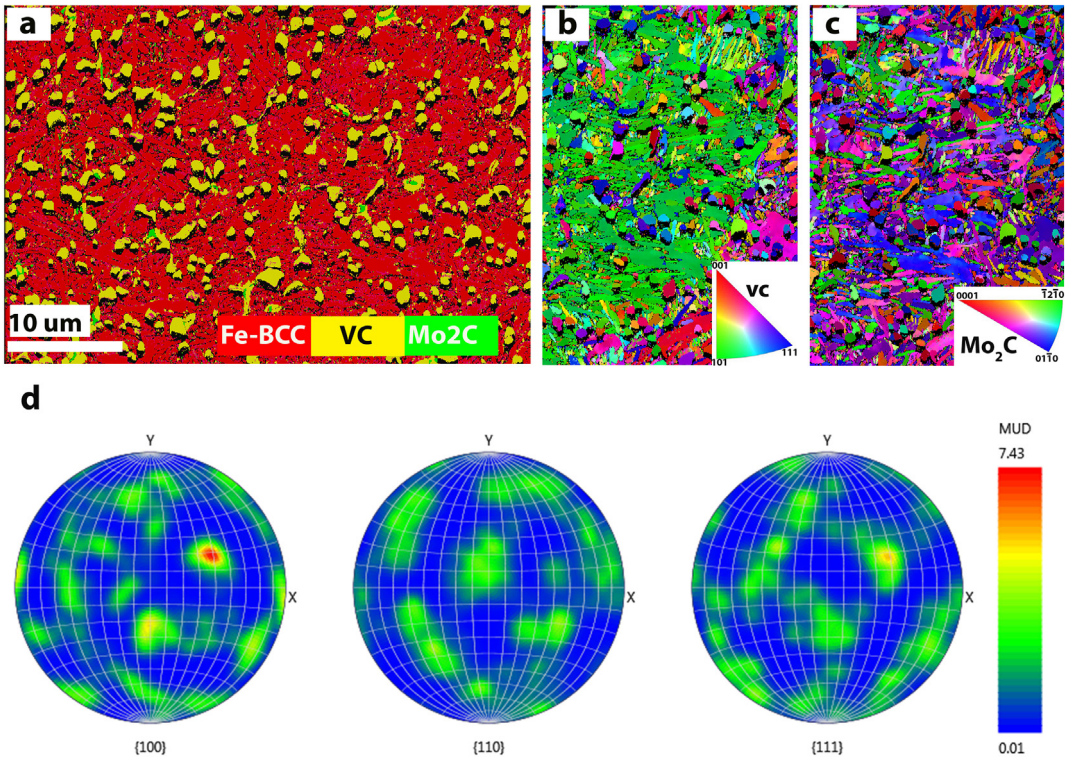

Fig. 6. (a) EBSD phase map of V-rich HSS 5 mm/s, (b) and (c) IPF showing the heterogeneous grain orientations and (d) PF of Fe-BCC for {100}, {110} and {111} planes.

4. Discussion

LMD of V-rich HSS alloy was performed at different laser scan speeds to modify the microstructural features to further investigate the effect of these modifications on high temperature wear. Although in hot metal forming, tools experience severe surface degradation due to thermo-mechanical fatigue and wear [33], however the current paper only addresses the high temperature wear.

Double layer clad samples of V-rich HSS were deposited at three different laser scanning speeds. It was found that by increasing the processing speed, the micro-hardness of the laser deposits increased from 750 HV to 835 HV. Increasing the processing speed, resulted in an increase in the cooling rate due to which the micro-hardness of the V-rich HSS was improved [34]. This increase in micro-hardness is due to the shorter interaction time between laser beam and the materials (powder particles and substrate), enhancing the cooling rate and subsequently providing a shorter time for the grains to grow [35]. Mellouli et al. [36] stated that increasing the micro-hardness of the hot-working tool steel increases the thermal fatigue strength by decreasing the crack growth. Sequential laser deposition also resulted in decreasing the micro-hardness of the previously deposited layer. Such a decease in the micro-hardness is mainly due to tempering of the existing lath martensite or yielding a softer martensite with low carbon contents and coarse carbide precipitates [37]. The micro-hardness plot of HSS laser deposits (Fig. 8) shows a gradual decrease in the micro-hardness which can be attributed to different degrees of tempering at different depths [38].

LMD of the V-rich HSS alloys at three different cooling rates (production speeds) produced microstructures with distinctive morphologies and different sizes of carbides, as shown in the BSE micrographs (Fig. 3). The phase fraction of carbides (VC carbides) was increased by increasing the laser processing speed as found in the EBSD analysis of the laser deposits. During the high temperature pin-on-disc tests of the V-rich HSS alloys, it was found that the friction profile of V-rich HSS 10 mm/s was stable during testing with a lower coefficient of friction ($\mu \approx 0.55$) compared to V-rich HSS 5 mm/s and 15 mm/s. The wear rates of V-rich 5 mm/s and 10 mm/s were comparable but the V-rich 15 mm/s resulted in slightly higher wear. The high temperature tribological behavior of the laser deposits depends integrally upon the microstructural features (matrix-carbides combined micro-hardness, phase

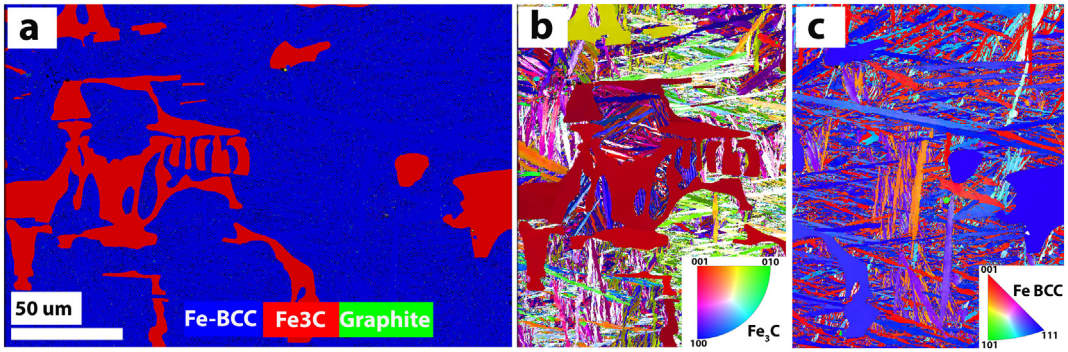

Fig. 7. (a) EBSD phase map of CE-ICDP iron, (b) and (c) IPF showing the heterogeneous grain orientations.

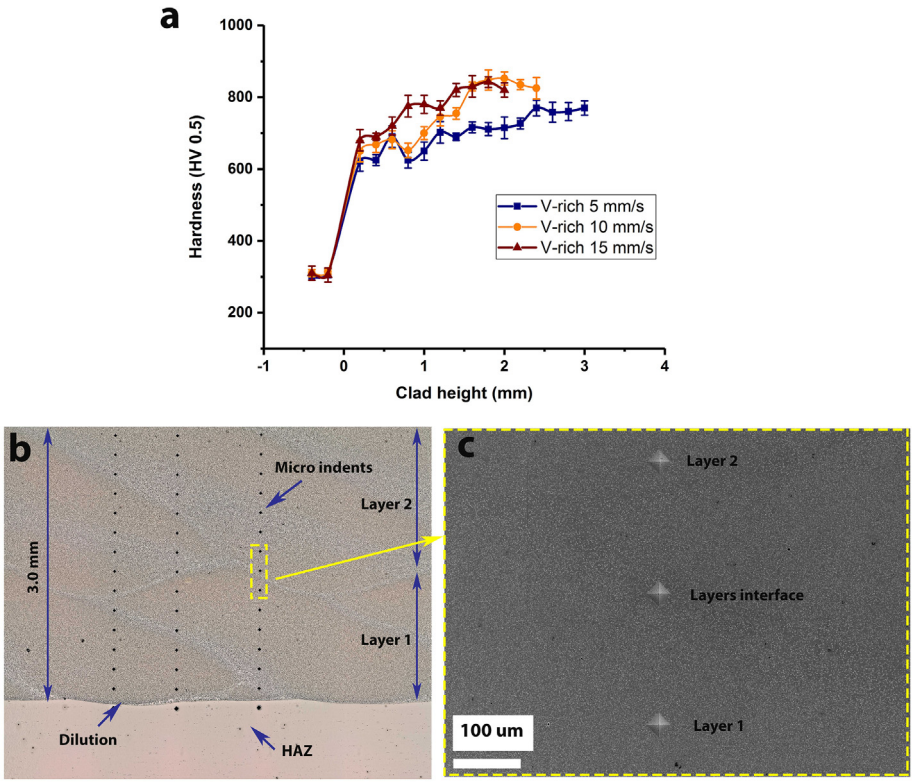

Fig. 8. (a) Micro-hardness plot of the laser deposited V-rich HSS alloy at 5, 10 and 15 mm/s, (b) optical image of the cross section of laser deposited V-rich HSS at 5 mm/s showing two overlapping clad layers with micro indents and (c) SEM image of the micro indents area highlighted in (b).

fraction of carbides, morphology and size of carbides) [39]. During the wear tests, pin was brought in contact with the pre-oxidized surface of counter disc (oxide-metal contact). The hard oxide layer of the disc abraded the V-rich HSS pin surface. Initial contact wore the relatively softer matrix of the HSS alloy and the contact load was supported by hard VC carbides. In the mean time, a protective oxide layer was formed on the matrix to resist the hard abrasive oxide layer of counter surface (oxide-oxide contact), reducing the overall wear during rest of the test.

It is widely accepted that for cast HSS alloys, due to larger difference between the micro-hardness of the coarse carbides and matrix, that the preferential wear of the latter is higher, and as a result a "gripping effect" space occurs with the counter surface during tribological contacts [40]. For LMD V-rich HSS, the carbide were highly refined and also were homogeneously distributed throughout the matrix. By increasing the matrix micro-hardness in V-rich 10 mm/s due to a faster cooling rate, the stability of the friction signal improved compared to that of V-rich 5 mm/s. Further increasing the cooling rates in V-rich 15 mm/s, refined the carbides further but again resulted in an unstable friction profile and also an increase in the wear. This shows that reducing the size of carbides below a certain limit also reduces their load bearing capability. In addition, morphology of the VC carbides was also changed from square and round shape to angular and rod-like shape in V-rich 15 mm/s, which is reported to be less effective against abrasive wear [19].

The surface of the LMD V-rich HSS was fully oxidized in all three cases (Figs. 11 and 12), providing protection from the hard oxide layer of the counter surface. However, abrasion marks on the matrix of the V-rich 15 mm/s were found (Fig. 10d), which could be due to limited support from the very fine angular and rod-like VC carbides during the contact. Joos et al. [41] reported that tribological behavior of HSS alloys at high temperature strongly depends on the oxidation, while

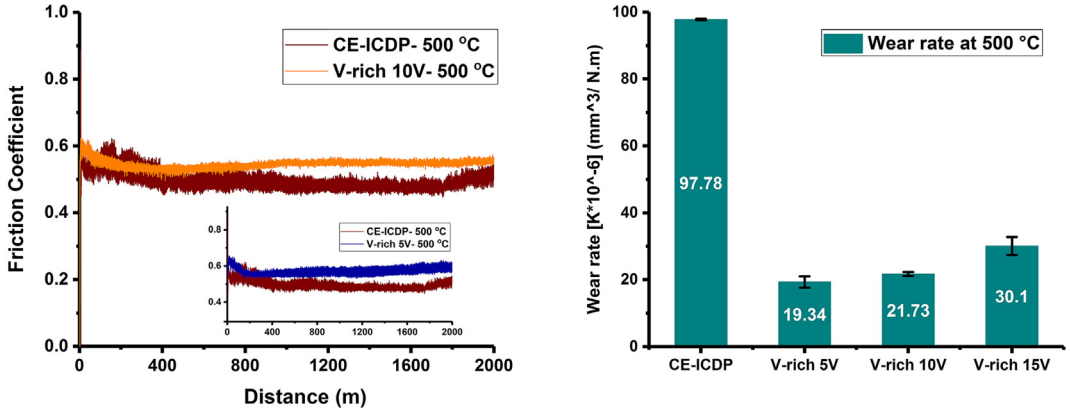

Fig. 9. (L) Comparison of friction profiles at 500 °C, insert: Comparative friction profile of V-rich HSS 5 mm/s and CE-ICDP iron, (R) plot showing a comparison of wear rates at 500 °C.

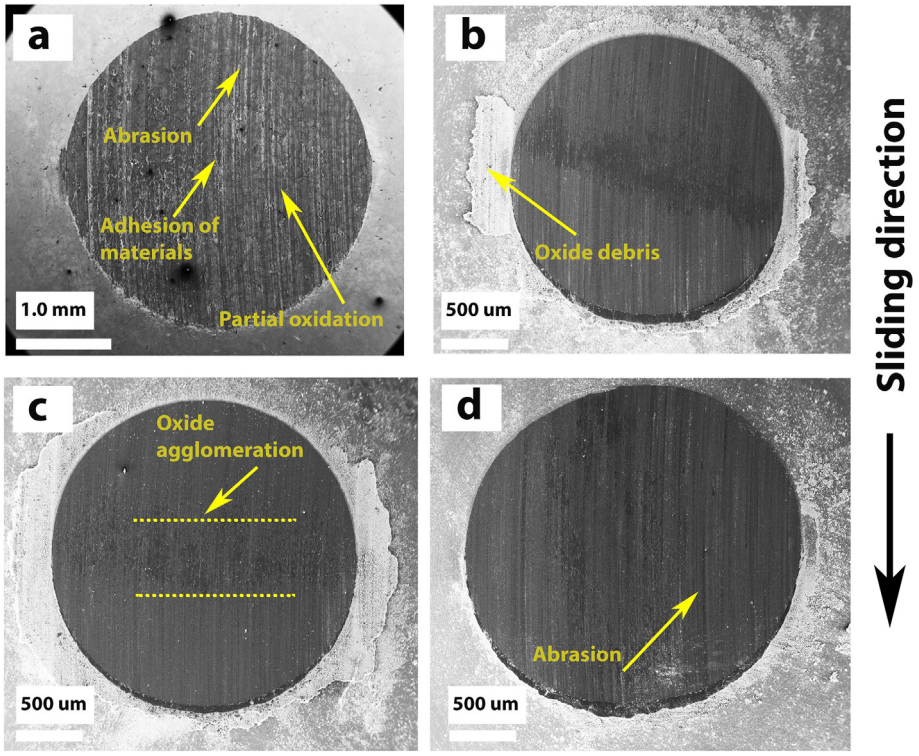

Fig. 10. SEM micrographs of worn surfaces of (a) CE-ICDP iron, (b) V-rich 5 mm/s, (c) V-rich 10 mm/s and (d) V-rich 15 mm/s.

oxidation itself depends on microstructure. Additionally, agglomeration and sintering of oxide debris were found at the center of V-rich HSS alloys. Examination of wear track of the counter surface showed a removal of oxide layer from almost middle of the wear track which was possibly adhered and transferred to the center of the pin surface [42].

High temperature pin-on-disc testing of CE-ICDP iron showed that

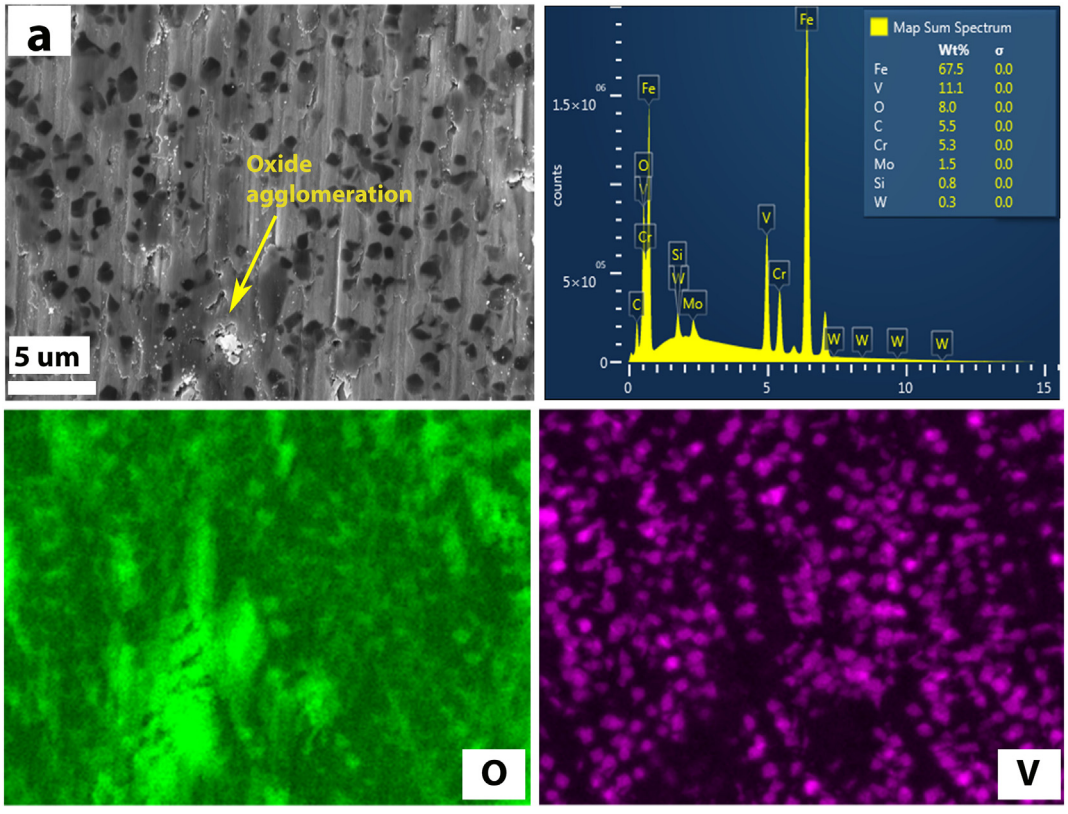

Fig. 11. (a) SEM micrograph of the worn surface of V-rich HSS 5 mm/s with the EDS spectrum showing 8% of the oxygen and EDS images showing the distribution of oxidation.

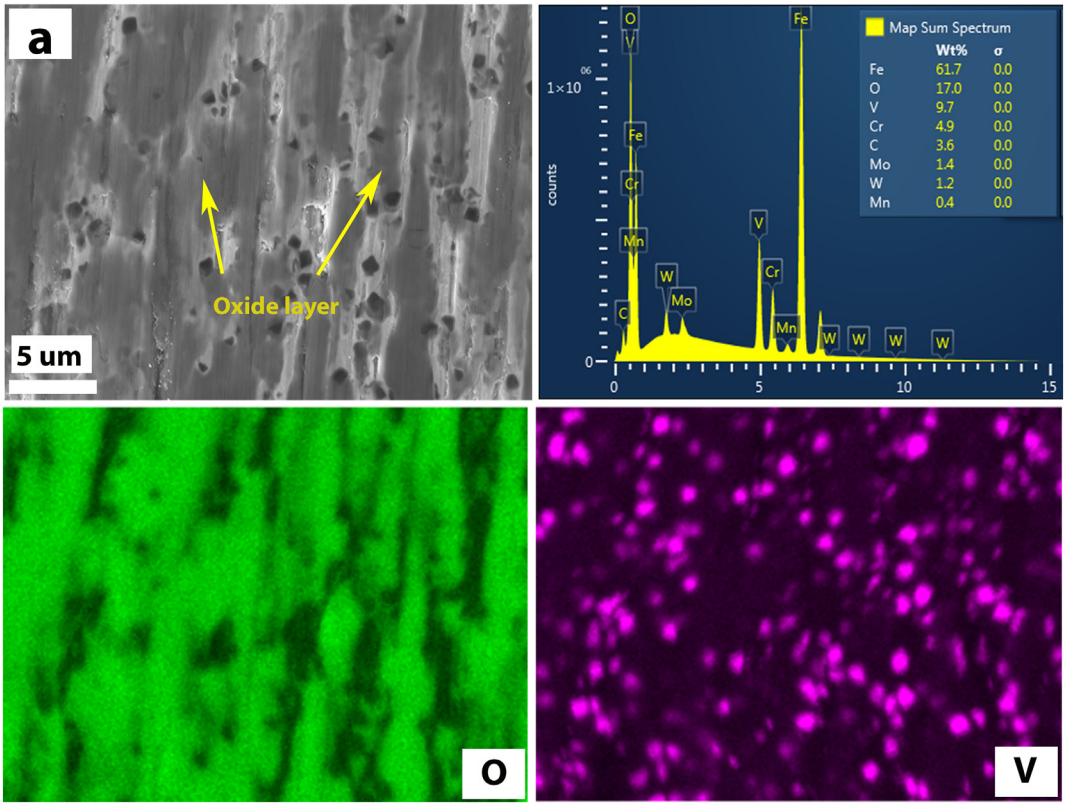

Fig. 12. (a) SEM micrograph at the center of the worn surface of V-rich HSS 5 mm/s with the EDS spectrum showing 17% of the oxygen and EDS images showing the distribution of oxidation.

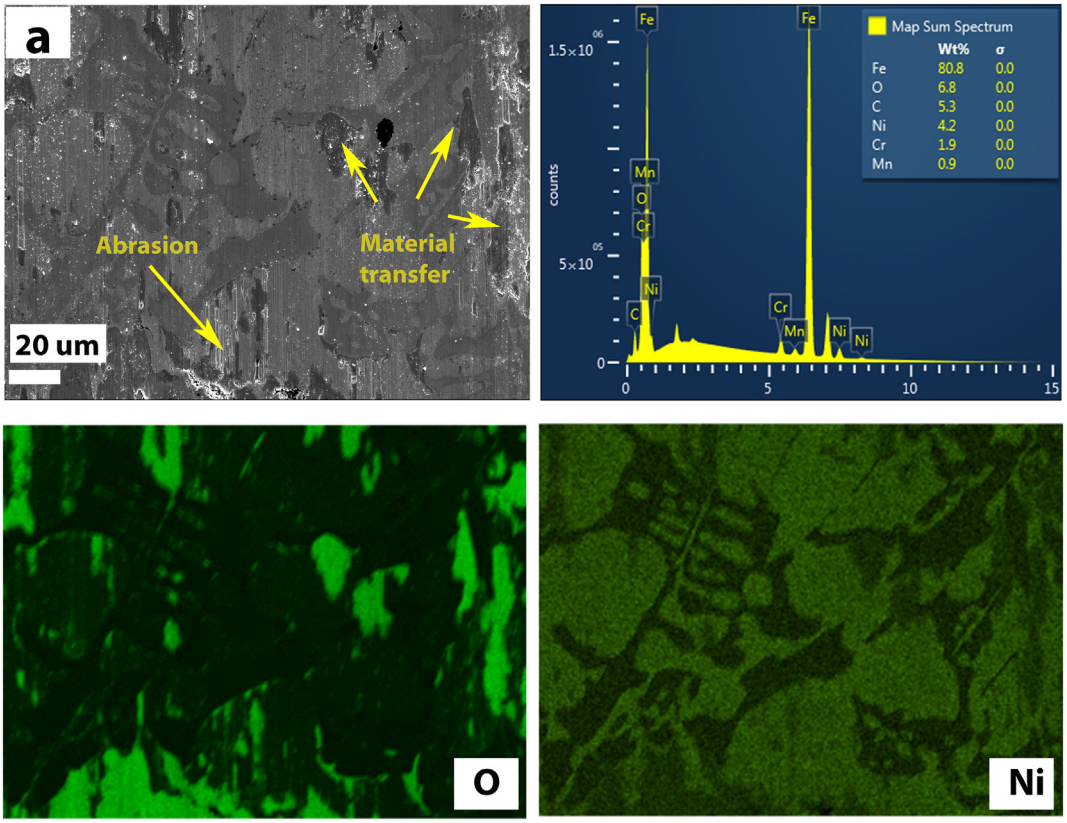

Fig. 13. (a) SEM micrograph of the worn surfaces of CE-ICDP iron with the EDS spectrum showing 7% of the oxygen and EDS images showing the distribution of oxidation.

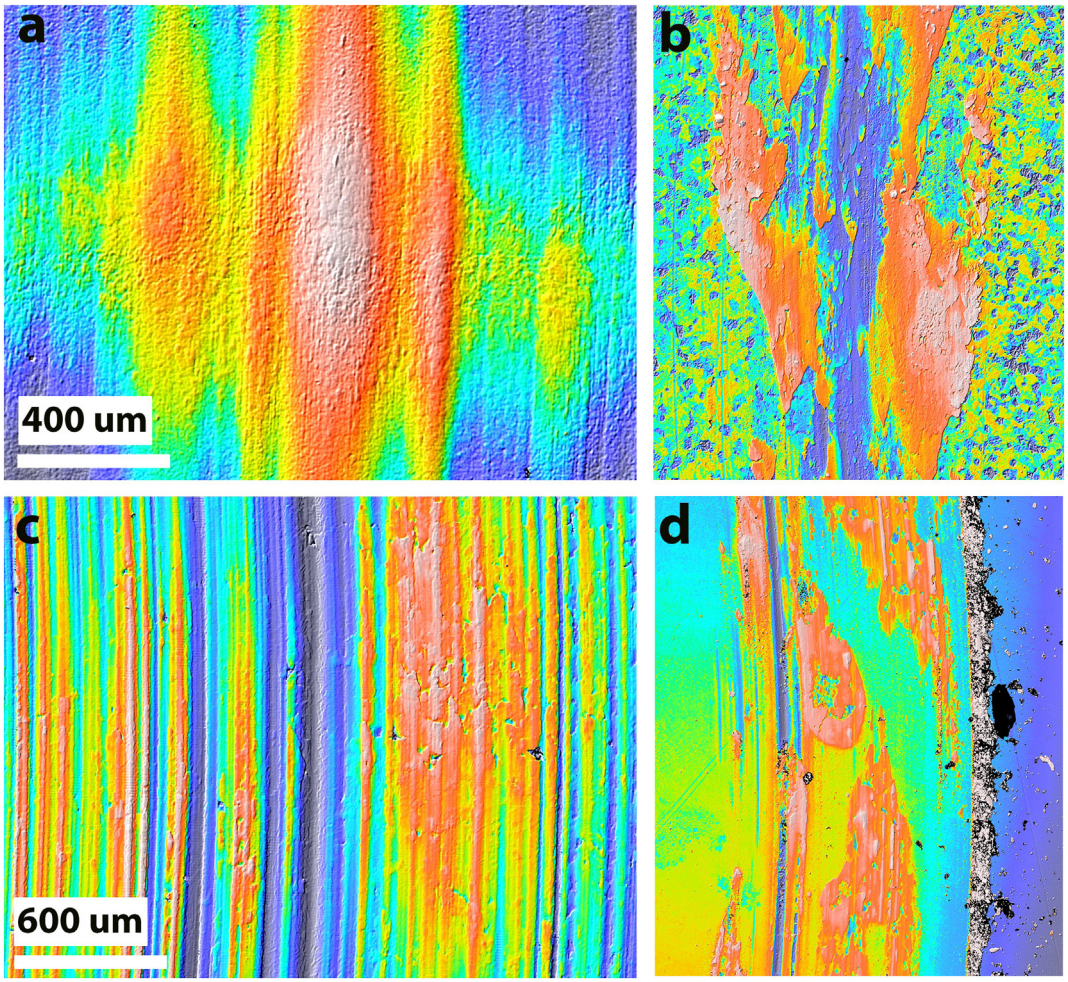

Fig. 14. Surface roughness plots of the worn surfaces of pins and discs, (a) V-rich HSS 10 mm/s and (b) counter disc, and (c) CE-ICDP iron pin and (d) counter disc.

cast iron alloy yielded 3–4 times higher wear compared to LMD V-rich HSS alloys. Although friction coefficient of the CE-ICDP iron was lower (≈0.5) but showed noise and fluctuations throughout the tests due to continuous abrasion and adhesion. The soft matrix and cementite were abraded by the hard oxide layer of the counter disc (Fig. 10). Partial oxide formation was found on the worn surface. Preferentially, metallic and oxide debris also promoted the three-body abrasion. Surface analysis showed the presence of abrasion grooves all over the worn surface, resulting in high surface roughness (Fig. 14c). The CE-ICDP iron is preferred in hot metal forming as CE-ICDP iron contain free graphite which is perceived to lubricate the contact between the CE-ICDP iron tool and counter surface to avoid sticking and micro-welding [28,43]. Sticking could result in the surface defects of tools and products [44,45]. On the contrary, SEM micrographs clearly indicated the presence of material transfer to the worn surface (Fig. 13) which could be due to low percentage of graphite (≈1–2%). Increasing the amount of graphite would worsen the wear resistance of CE-ICDP iron due to further softening.

Due to the complex interaction between various microstructural, mechanical and process variables affecting tribological performance of LMD V-rich HSS alloys and cast CE-ICDP iron at 500 °C, a collective-qualitative analysis is presented in a rating plot, see Fig. 15. Five dominant variables (wear resistance, stable friction profile, carbide morphology/size, carbide phase fraction and micro-hardness) are rated from 1 to 5; with 5 being the best. The collective-qualitative analysis rated LMD V-rich HSS 10 mm/s the highest, suggesting it to be the most suitable alloy in the light of the considered variables.

Considering the friction and wear performance of cast CE-ICDP iron,

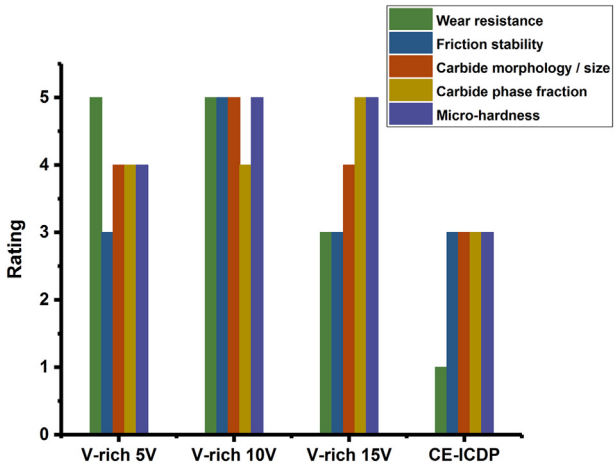

Fig. 15. A collective-qualitative rating plot of the LMD V-rich HSS alloys and cast CE-ICDP iron.

it can be concluded that LMD HSS alloys enriched with VC carbides could be a better choice for such high temperature applications. However, the impact of sequential laser deposition on the micro-hardness should be addressed by strengthening the solid solution to avoid softening of martensite. Further, additions of soft phases (self-lubricating materials) will enhance the wear performance of LMD V-rich HSS [46,47] by avoiding adhesion to the counter material [48].

5. Conclusions

LMD deposition of V-rich HSS alloy was performed by varying the laser scan speed. Conclusions drawn based on this production methodology, comprehensive microstructural analysis and comparative high temperature pin-on-disc wear testing with conventional spun cast CE-ICDP iron are listed below.

(1) Due to high cooling rates in LMD, the resulting microstructure of V-rich HSS was highly refined as compared to the conventional casting processes.
(2) Laser processing of V-rich HSS alloy at three different laser scan speeds, produced three different microstructures. Increasing the laser scan speed changed the morphology of VC carbides from square and round shape to angular and rod-like shape. Micro-hardness (HV 0.5) was increased from 760 HV to 835 HV.
(3) Sequential laser deposition drastically affected the micro-hardness of the previously deposited layer. This was due to the tempering of existing martensite and yielding a softer martensite.
(4) High temperature wear mechanisms have been found to be a combination of abrasive, adhesive and oxidative wear present for all samples, with the latter being dominant.
(5) High temperature tribological behavior of the LMD V-rich HSS depends upon the combined effect of microstructural features and average matrix-carbides micro-hardness.
(6) V-rich HSS 10 mm/s showed a stable friction profile compared to that of V-rich HSS 5, 15 mm/s and CE-ICDP iron.
(7) VC carbides provide load carrying capability during wear. However, reducing the size of VC carbides below a certain limit (as in V-rich HSS 15 mm/s), reduces their ability to provide such mechanical support.
(8) CE-ICDP iron showed ≈3–4 times higher wear compared to LMD V-rich HSS alloys. SEM and EDS images of the worn surfaces showed partial signs of oxidation due to continuous abrasion.

Acknowledgments

This Project is funded by the European Research Fund for Coal and Steel (RFCS) under the grant agreement no. RFSR-CT-2015-00009. The authors are highly grateful to Dirk Wanders, Leo Tiemersma and Erik de Vries from the University of Twente (Enschede, the Netherlands) for assisting in laser metal fabrication and wear testing.

References

[1] M.S. Gök, Y. Küçük, A. Erdoğan, M. Öge, E. Kanca, A. Günen, Dry sliding wear behavior of borided hot-work tool steel at elevated temperatures, Surface and Coatings Technology 328 (2017) 54–62.
[2] Premendra, L. Philippe, H. Terryn, J. de Wit, L. Katgerman, Understanding the electrochemical, microstructural and morphological changes during hot rolling from a corrosion perspective, Surface and Coatings Technology 201 (2006) 828–834.
[3] A.K. Tieu, Q. Zhu, H. Zhu, C. Lu, An investigation into the tribological behaviour of a work roll material at high temperature, Wear 273 (2011) 43–48.
[4] C. Meng, H. Zhou, Y. Zhou, M. Gao, X. Tong, D. Cong, C. Wang, F. Chang, L. Ren, Influence of different temperatures on the thermal fatigue behavior and thermal stability of hot-work tool steel processed by a biomimetic couple laser technique, Optics & Laser Technology 57 (2014) 57–65.
[5] K.C. Hwang, S. Lee, H.C. Lee, Effects of alloying elements on microstructure and fracture properties of cast high speed steel rolls: part I: microstructural analysis, Materials Science and Engineering: A 254 (1998) 282–295.
[6] H. Phan, A. Tieu, H. Zhu, B. Kosasih, Q. Zhu, A. Grima, T. Ta, A study of abrasive wear on high speed steel surface in hot rolling by discrete element method, Tribology International 110 (2017) 66–76.
[7] Y. Sano, T. Hattori, M. Haga, Characteristics of high-carbon high speed steel rolls for hot strip mill, ISIJ International 32 (1992) 1194–1201.
[8] S. Lee, D.O. Hyung Kim, J.H. Ryu, K. Shin, Correlation of microstructure and thermal fatigue property of three work rolls, Metallurgical and Materials Transactions A: Physical Metallurgy and Materials Science 28 (1997) 2595–2608.
[9] C. Kwok, F. Cheng, H. Man, Microstructure and corrosion behavior of laser surface-melted high-speed steels, Surface and Coatings Technology 202 (2007) 336–348.
[10] F. Belzunce, A. Ziadi, C. Rodriguez, Structural integrity of hot strip mill rolling rolls, Engineering Failure Analysis 11 (2004) 789–797.
[11] X. Yu, Z. Jiang, J. Zhao, D. Wei, J. Zhou, C. Zhou, Q. Huang, The role of oxide-scale microtexture on tribological behaviour in the nanoparticle lubrication of hot rolling, Tribology International 93 (2016) 190–201.
[12] M. Nilsson, M. Olsson, Microstructural, mechanical and tribological characterisation of roll materials for the finishing stands of the hot strip mill for steel rolling, Wear 307 (2013) 209–217.
[13] L. Dubourg, J. Archambeault, Technological and scientific landscape of laser cladding process in 2007, Surface and Coatings Technology 202 (2008) 5863–5869.
[14] N. Shamsaei, A. Yadollahi, L. Bian, S.M. Thompson, An overview of direct laser deposition for additive manufacturing; part II: mechanical behavior, process parameter optimization and control, Additive Manufacturing 8 (2015) 12–35.
[15] G. Sun, S. Yao, Z. Wang, X. Shen, Y. Yan, R. Zhou, Z. Ni, Microstructure and mechanical properties of HSLA-100 steel repaired by laser metal deposition, Surface and Coatings Technology 351 (2018) 198–211.
[16] V. Ocelík, M. Eekma, I. Hemmati, J. De Hosson, Elimination of start/stop defects in laser cladding, Surface and Coatings Technology 206 (2012) 2403–2409.
[17] E. Toyserkani, A. Khajepour, S. Corbin, Laser Cladding, vol. 119, (2004).
[18] N.U. Rahman, M.B. De Rooij, D.T.A. Matthews, G. Walmag, M. Sinnaeve, G.R.B.E. Römer, Wear characterization of multilayer laser cladded high speed steels, Tribology International 130 (2019) 52–62.
[19] N. Hashemi, A. Mertens, H.M. Montrieux, J.T. Tchuindjang, O. Dedry, R. Carrus, J. Lecomte-Beckers, Oxidative wear behaviour of laser clad high speed steel thick deposits: influence of sliding speed, carbide type and morphology, Surface and Coatings Technology 315 (2017) 519–529.
[20] A. Molinari, M. Pellizzari, A. Biggi, G. Corbo, A. Tremea, Primary carbides in spincast HSS for hot rolls and their effect on the oxidation behaviour, 6th International Tooling Conference. Karlstad, Sweden, (2002), pp. 437–452.
[21] L. Xu, S. Wei, F. Xiao, H. Zhou, G. Zhang, J. Li, Effects of carbides on abrasive wear properties and failure behaviours of high speed steels with different alloy element content, Wear 376–377 (2017) 968–974.
[22] E. Luc, M. Bigerelle, R. Deltombe, M. Dubar, The representative topography of worn hot rolling mill cylinders, Tribology International 82 (2015) 387–399.
[23] N.F. Garza-Montes-de Oca, W.M. Rainforth, Wear mechanisms experienced by a work roll grade high speed steel under different environmental conditions, Wear 267 (2009) 441–448.
[24] N.U. Rahman, L. Capuano, A. Van Der Meer, M.B. De Rooij, D.T.A. Matthews, G. Walmag, M. Sinnaeve, A. Garcia-Junceda, M. Castillo, G.R.B.E. Römer, Development and characterization of multilayer laser cladded high speed steels, Additive Manufacturing 24 (2018) 76–85.
[25] J.F. Archard, Contact and rubbing of flat surfaces, Journal of Applied Physics 24 (1953) 981–988.
[26] I. Hemmati, V. Ocelik, J.T.M. De Hosson, The effect of cladding speed on phase constitution and properties of AISI 431 stainless steel laser deposited coatings, Surface and Coatings Technology 205 (2011) 5235–5239.
[27] K. Rutherford, I. Hutchings, A micro-abrasive wear test, with particular application to coated systems, Surface and Coatings Technology 79 (1996) 231–239.
[28] T. Valek, J. Hampl, Prediction of metallurgic quality of ICDP material before tapping, Physics Procedia 22 (2011) 191–196.
[29] E. Luc, M. Bigerelle, R. Deltombe, M. Dubar, The representative topography of worn hot rolling mill cylinders, Tribology International 82 (2015) 387–399.
[30] Y. Herrera, I. Grigorescu, J. Ramirez, C. Di Rauso, M. Staia, Microstructural characterization of vanadium carbide laser clad coatings, Surface and Coatings Technology 108–109 (1998) 308–311.
[31] X. Fan, Z. Yang, C. Zhang, Y. Zhang, H. Che, Evaluation of vanadium carbide coatings on AISI H13 obtained by thermo-reactive deposition/diffusion technique, Surface and Coatings Technology 205 (2010) 641–646.
[32] Y. Yin, J. Sun, S. Teng, C. Niu, Oxidation behavior of high-speed steel used for hot rolls, Oxidation of Metals 86 (2016) 45–57.
[33] D. Benasciutti, E. Brusa, G. Bazzaro, Finite elements prediction of thermal stresses in work roll of hot rolling mills, Procedia Engineering 2 (2010) 707–716.
[34] S.N. Aqida, D. Brabazon, S. Naher, An investigation of phase transformation and crystallinity in laser surface modified H13 steel, Applied Physics A 110 (2013) 673–678.
[35] X.H. Wang, M. Zhang, L. Cheng, S.Y. Qu, B.S. Du, Microstructure and wear properties of in situ synthesized VC carbide reinforced Fe-based surface composite coating produced by laser cladding, Tribology Letters 34 (2009) 177–183.
[36] D. Mellouli, N. Haddar, A. Köster, H.F. Ayedi, Hardness effect on thermal fatigue damage of hot-working tool steel, Engineering Failure Analysis 45 (2014) 85–95.
[37] G. Telasang, J. Dutta Majumdar, G. Padmanabham, I. Manna, Structure-property correlation in laser surface treated AISI H13 tool steel for improved mechanical properties, Materials Science and Engineering: A 599 (2014) 255–267.
[38] G. Telasang, J. Dutta Majumdar, G. Padmanabham, M. Tak, I. Manna, Effect of laser parameters on microstructure and hardness of laser clad and tempered AISI H13 tool steel, Surface and Coatings Technology 258 (2014) 1108–1118.
[39] S.H. Wang, J.Y. Chen, L. Xue, A study of the abrasive wear behaviour of laser-clad tool steel coatings, Surface and Coatings Technology 200 (2006) 3446–3458.
[40] M. Pellizzari, D. Cescato, M.G. De Flora, Hot friction and wear behaviour of high speed steel and high chromium iron for rolls, Wear 267 (2009) 467–475.
[41] O. Joos, C. Boher, C. Vergne, C. Gaspard, T. Nylen, F. Rezaï-Aria, Assessment of oxide scales influence on wear damage of HSM work rolls, Wear 263 (2007) 198–206.
[42] H. Zhu, Q. Zhu, A.K. Tieu, B. Kosasih, C. Kong, A simulation of wear behaviour of high-speed steel hot rolls by means of high temperature pin-on-disc tests, Wear 302 (2013) 1310–1318.
[43] L. Hao, H. Wu, D. Wei, X. Cheng, J. Zhao, S. Luo, L. Jiang, Z. Jiang, Wear and

friction behaviour of high-speed steel and indefinite chill material for rolling ferritic stainless steels, Wear 376–377 (2017) 1580–1585.
[44] D. Wei, J. Huang, A. Zhang, Z. Jiang, A. Tieu, X. Shi, S. Jiao, The effect of oxide scale of stainless steels on friction and surface roughness in hot rolling, Wear 271 (2011) 2417–2425.
[45] M. Wei, S. Wang, L. Wang, X. Cui, K. Chen, Effect of tempering conditions on wear resistance in various wear mechanisms of H13 steel, Tribology International 44 (2011) 898–905.
[46] H. Torres, T. Vuchkov, S. Slawik, C. Gachot, B. Prakash, M. Rodríguez Ripoll, Self-lubricating laser claddings for reducing friction and wear from room temperature to 600 °C, Wear 408–409 (2018) 22–33.
[47] H. Torres, T. Vuchkov, M. Rodríguez Ripoll, B. Prakash, Tribological behaviour of MoS2-based self-lubricating laser cladding for use in high temperature applications, Tribology International 126 (2018) 153–165.
[48] J. Beese, Lubrication of hot-strip-mill rolls, Wear 23 (1973) 203–208.